

# The preamplifier-shaper for the ALICE TPC-Detector

H. K. Soltveit<sup>1a</sup>, J. Stachel<sup>a</sup>, P. Braun-Munzinger<sup>b</sup>, L. Musa<sup>c</sup>, H. A. Gustafsson<sup>†d</sup>, U. Bonnes<sup>e</sup>, H. Oeschler<sup>e</sup>, L. Osterman<sup>d</sup>, S. Lang<sup>e</sup>, for the ALICE TPC Collaboration

<sup>a</sup>*Physikalisches Institut, Ruprecht-Karls-Universität Heidelberg, Heidelberg, Germany*

<sup>b</sup>*GSI Helmholtzzentrum für Schwerionenforschung GmbH, Darmstadt, Germany*

<sup>c</sup>*European Organization for Nuclear Research (CERN), Geneva*

<sup>d</sup>*Division of Experimental High Energy Physics, University of Lund, Lund, Sweden*

<sup>e</sup>*Institut für Kernphysik, Technische Universität Darmstadt, Darmstadt, Germany*

---

## Abstract

In this paper the PreAmplifier ShAper (PASA) for the Time Projection Chamber (TPC) of the ALICE experiment at LHC is presented. The ALICE TPC PASA is an ASIC that integrates 16 identical channels, each consisting of Charge Sensitive Amplifiers (CSA) followed by a Pole-Zero network, self-adaptive bias network, two second-order bridged-T filters, two non-inverting level shifters and a start-up circuit. The circuit is optimized for a detector capacitance of 18-25 pF. For an input capacitance of 25 pF, the PASA features a conversion gain of 12.74 mV/fC, a peaking time of 160 ns, a FWHM of 190 ns, a power consumption of 11.65 mW/ch and an equivalent noise charge of  $244e + 17e/pF$ . The circuit recovers smoothly to the baseline in about 600 ns. An integral non-linearity of 0.19% with an output swing of about 2.1 V is also achieved. The total area of the chip is 18 mm<sup>2</sup> and is implemented in AMS's C35B3C1 0.35 micron CMOS technology. Detailed characterization test were performed on about 48000 PASA circuits before mounting them on the ALICE TPC front-end cards. After more than two years of operation of the ALICE TPC with p-p and Pb-Pb collisions, the PASA has demonstrated to fulfill all requirements.

---

## 1. Introduction

The Time Projection Chamber (TPC) is the main tracking detector in the central barrel of the ALICE experiment [1] at the CERN LHC. It is a 90 m<sup>3</sup> cylinder filled with gas and divided in two drift regions by the central electrode located at its axial center. A field cage creates a uniform electric field along each half of the chamber.

---

<sup>1</sup>Corresponding author, e-mail:soltveit@physi.uni-heidelberg.de

Charged particles traversing the TPC volume ionize the gas along their paths liberating electrons that drift toward the end plates of the chamber. The necessary signal amplification is provided through avalanche effects in the vicinity of the anode wires. Moving from the anode wire toward the surrounding electrodes, the positive ions created in the avalanche induce a positive current signal which is characterized by a fast rise time (less than 1 ns) and a long tail with a rather complex shape. It carries a charge that for the minimum ionizing particle is in the order of 4.8 fC. The readout of the signal is done by the 557 568 pads that form the cathode plane of the conventional wire chambers located at the TPC end caps. The amplitude, which is different for the different pad sizes, has a typical value of 7  $\mu$ A. The signal is delivered on the detector impedance which, to a very good approximation, is a pure capacitance of the order of 12 pF.

The signals from the pads are passed to 4356 front-end cards, located about 10 cm away from the pad plane, via flexible kapton cables. In the front-end card the charge-sensitive shaping amplifier of the PASA circuit transforms the charge induced in the pads into a differential semi-Gaussian signal that is fed to the input of the ALTRO chip [2].

This paper addresses the design of the PASA that is fabricated in a 0.35 micron CMOS technology. In section 2, the used PASA architecture is presented. This architecture consists of several blocks that are described in sections 3, 4, 5, and 6. In section 7 the layout techniques are explained. In section 8, the performance of the chip at the simulation level is shown. The standalone test results of all produced chips and their performance in the final system are described in section 9. The conclusions are presented in section 10.

## 2. ALICE TPC PASA overview

The list of requirements given as guideline prior to the design of the PASA is presented in Table 1. A simplified block diagram of the PASA signal processing chain developed in order to fulfill them is shown in Fig. 1. The ASIC

Parameter	Specification
Noise	< 1000e
Shaping time (ns)	190
Non-linearity	< 1%
Crosstalk	< 0.3%
Total max capacitance (pF)	25
Conv. gain (mV/fC)	12
Power con.(mW/ch)	< 20

Table 1: List of requirements given for the design of the ALICE TPC PASA.

has 16 equal channels, consisting of a ESD network made of six diodes and a

50  $\Omega$  resistor, a positive polarity Charge Sensitive Amplifier (CSA) with a capacitive feedback  $C_f$  and a resistive feedback  $R_f(M_f)$  connected in parallel, a Pole-Zero Cancellation (PZC) network, a self-adaptive bias network, a CR filter and two  $(RC)^2$  bridged-T filters, a Common-Mode Feed-Back network (CMFB) and two quasi-differential gain-2 amplifiers. Not shown in the block diagram is the internal bias-network.

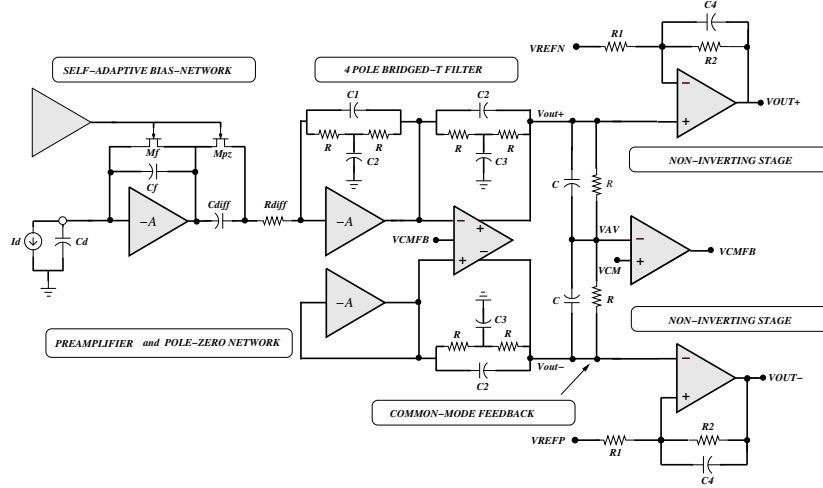


Figure 1: A simplified block diagram of the PreAmplifier-ShAper (PASA) signal processing chain.

Since the charge  $Q_{in}$  delivered by the TPC detector readout chambers is very small (typically  $7\mu A$ ), and short (1ns), it is unsuitable for immediate signal processing. Therefore, the input signal is first integrated and amplified by the CSA producing at its output a voltage signal  $V_{out}$ , whose amplitude is proportional to the total charge  $Q_{in}$  and characterized by a long decay time constant, which is defined by the feedback network parameters ( $\tau = R_f(M_f) \cdot C_f = 4.2 \mu s$ ) of the CSA:

$$V_{out} = \frac{Q_{in}}{C_f} \cdot \exp(-t/\tau) \quad (1)$$

As seen in Fig. 1 and mathematically represented in Eq. 1 a NMOS transistor  $R_f(M_f)$  operated in the subthreshold region is connected in parallel to the feedback capacitor  $C_f$ . The purpose of this transistor is to avoid saturation of the CSA, by continuously discharging the feedback capacitance  $C_f$ . As later explained in section 3, this transistor will contribute to the parallel noise at the CSA input. Therefore, in order to limit its noise contribution, it was chosen to be a high value ( $10M\Omega$ ) as a compromise between noise and count rate. The relatively big resistance value chosen here, was implemented as an active feedback transistor instead of as a passive resistor, that otherwise would have increased the area, parasitic capacitances, speed and noise.

To operate a transistor with such a high resistance makes its drain-to-source resistance  $R_{ds}$  sensitive to process, temperature and bias conditions. To neutralize this sensitivity the self-adaptive bias-network developed by [3] was adopted. This scheme has the advantage that it keeps the difference  $V_g(Mf)-V_{in}(M1)$  constant, making  $R_f(Mf)$  independent of the effects mentioned above.

Still, the relatively long discharge time constant of the CSA makes it vulnerable to pile-up. The low frequency part of the pulse is then removed by the  $C_{diff}R_{diff}$ -filter stage. Due to the exponential decay of the CSA feedback network in combination with the differentiator network, an undershoot is created at the shaper output with the same time constant as the CSA of  $\tau = R_f(Mf)*C_f$ . This undershoot was removed by creating a PZC circuit by adding a transistor  $R_{pz}$  ( $M_{pz}$ ) in parallel to the capacitor  $C_{diff}$  in the differentiator stage. This creates a Zero in the transfer function that cancels the low frequency pole introduced by the CSA feedback network. In order to ensure that the Zero introduced by the network  $M_{pz}-C_{diff}$  adapts dynamically and accurately cancels the pole associated with the CSA feedback network  $C_f-M_f(R_f)$ , the gate voltage of the transistor  $M_{pz}(R_{pz})$  is controlled by the same self-adaptive bias-network as the  $M_f(R_f)$  transistor.

To improve the linearity of the charge to voltage gain, a voltage divider was inserted between the output of the preamplifier and the source of  $M_f$  [4]. This reduces the variation for  $R_f(M_f)$  during the operation. Moreover,  $t_{decay} = k*R_f(M_f)*C_f$  is increased by the factor  $k = (R_1+R_2)/R_2$ , resulting in a very precise return to the baseline. Owing to the method described above, the maximum undershoot created by the mismatch of the components due to the variation of the CMOS process parameters, never exceed the 0.1% of the circuit dynamic range.

The output signal of the CSA and the PZC network is then amplified and shaped by two  $2^{nd}$  order bridged-T filters (see section 4) to optimize the signal-to-noise ratio (SNR) and to limit the signal bandwidth.

The shaped signal is then fed to the last stage consisting of two non-inverting stages (see section 5), built around a Miller operational amplifier, each providing a fixed gain of 2.

To adapt to the ALTRO input dynamic range, the two output DC levels  $V_{OUT+}$  and  $V_{OUT-}$  are defined by three externally given references,  $V_{REFN}$  (0.56 V),  $V_{REFP}$  (1.056 V) and  $V_{CM}$  (1.056 V).

### 3. The core amplifier

The core amplifier topology and the input transistor (PMOS versus NMOS) are key choices in the design of a low-power low-noise charge sensitive amplifier, since they typically represent the largest contribution to the total power dissipation and the overall system noise. The chosen topology (Fig. 2) is based on a single-ended folded cascode amplifier followed by a source follower. Owing to the short shaping time (190 ns), the white noise is the dominating source.

Therefore, an NMOS transistor was the natural choice, since it gives a higher transconductance  $gm$  and therefore better noise than a PMOS transistor under equal conditions.

The CSA has been optimized for a detector capacitance of 25 pF. The chosen aspect ratio (W/L) for the NMOS input transistor M1 of 2400/0.3 were based on the theoretical calculations described in subsection 3.1.

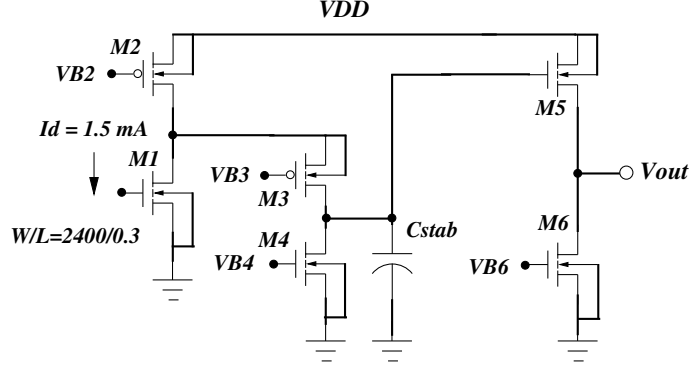


Figure 2: A schematic diagram of the Charge Sensitive Amplifier (CSA).

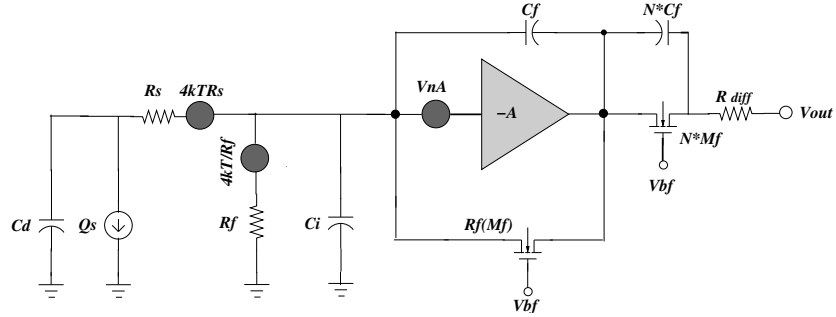


Figure 3: Block schematic of the CSA including pole-zero network and dynamic capacitance  $C_i$ .

To avoid cross-talk between adjacent channels, which can deteriorate the energy and position resolution, the input impedance ( $Z_{in}$ ) is made as small as possible. In this case it is calculated by using:

$$Z_{in} = \frac{C_{out}}{gm \cdot C_f} \quad (2)$$

where the feedback capacitance  $C_f$  is 0.42 pF, the capacitance  $C_{out}$  of the dominant pole is 1.4 pF and the input of the amplifier has a  $gm$  of 33 mS. This gives an effective input impedance of about 100  $\Omega$ .

The open-loop gain of this stage is 80 dB and the power consumption is about 6 mW.

### 3.1. Noise optimization of the PASA

In order to fulfill the requirement of a signal-to-noise ratio of 30:1 for the signal of 4.8fC produced by a MIP, the PASA has to feature a maximum noise of 1000 e. Noise here is referred to as equivalent noise Charge (ENC) which can directly be compared to the number of electrons created in the detector at the input of the CSA.

The noise model circuit for the PASA is shown in Fig. 3, where the three most important noise sources are represented as red dots. These are the series thermal noise ( $4kTR_s$ ) from the ESD protection circuit ( $70 \Omega$ ), the parasitic bulk resistance noise, the gate resistance thermal noise, the thermal channel noise ( $VnA$ ) from the input transistor M1, the flicker noise from the input transistor M1 and the parallel thermal noise contribution ( $4kT/R_f$ ) from the feedback transistor  $R_f$  ( $M_f$ ).

From the given specifications four main parameters are fixed: the shaping time  $\tau$ , the total detector capacitance  $C_T$ , the noise at 25 pF, the filter order ( $n=4$ ), and the power consumption. In addition, a series resistance of  $70 \Omega$  in the ESD network was chosen.

Therefore, to find the optimum  $ENC_T$ , the minimum gate length of transistor M1 available from the technology was chosen to achieve a high  $gm$ , a low thermal noise, a low power and a high speed. Given the parameters mentioned above, the only free parameter left is the width  $W$  of the input transistor M1.

Since the PASA performs a CR-RC<sup>4</sup> semi-Gaussian shaping, the relative ENC contributions from the four dominating and uncorrelated noise sources can then be expressed as [5]:

$$ENC_{R_s}^2 = 4kTR_s \frac{C_T^2 B(\frac{3}{2}, n - \frac{1}{2}) n}{4\pi\tau_s} \left( \frac{n!e^{2n}}{n^{2n}} \right) \quad (3)$$

$$ENC_{R_{fb}}^2 = \frac{4kT}{R_{fb}} \tau_s \frac{B(\frac{3}{2}, n - \frac{1}{2}) n}{4\pi} \left( \frac{n!e^{2n}}{n^{2n}} \right) \quad (4)$$

$$ENC_{th}^2 = \frac{8}{3} kT \frac{1}{gm} \frac{C_T^2 B(\frac{3}{2}, n - \frac{1}{2}) n}{q^2 4\pi\tau_s} \left( \frac{n!^2 e^{2n}}{n^{2n}} \right) \quad (5)$$

$$ENC_{\frac{1}{f}}^2 = \frac{K_f}{C_{ox}^2 WL} \frac{C_T^2}{q^2 2n} \left( \frac{n!^2 e^{2n}}{n^{2n}} \right) \quad (6)$$

where  $k$  is Boltzmann constant,  $T$  is the temperature (Kelvin),  $gm$  is the transconductance for the input transistor (mS),  $K_f$  is (Flicker noise coefficient),  $B(X, Y)$  is the Beta function [5], and  $C_T$  is the total capacitance at the input of M1.  $C_T = C_p + C_f + C_{gs} + C_{gd} + C_{FE-board}$ , where  $C_p$  is the pad capacitance,  $C_f$  is the feedback capacitance,  $C_{gs}$  and  $C_{gd}$  are the gate-source and gate-drain

capacitance of M1, respectively, and  $C_{FE-board}$  is the capacitance of the traces on the board.

Eq. (3) represents the noise contribution from the series resistance of the ESD network and its parasitic resistances. The parasitic resistances include the resistive poly-gate and the distributed substrate resistance. The main contributor here is the current limited resistor  $R_s$  of 70  $\Omega$  implemented in the ESD network. Its size was chosen as a compromise between noise and protection capability. This resistor produces a thermal noise voltage that is converted to a “noise charge” which at the output of the CSA gives a signal proportional to the charge flowing into the CSA. As mentioned above, the parasitic resistances related to the resistive poly-gate and the distributed substrate resistance also have an impact on the noise. However, the most important potential contributor and the only one that will be discussed here is the resistive poly-gate of the input transistor. This could, if not taken into consideration, introduce a noise equal to the resistance given by [5]

$$R_G = \frac{R_i}{12n} \quad (7)$$

where  $R_i$  is the resistance of the single poly-stripe of the width of the input transistor M1 and  $n$  is the number of poly-strips. As seen in Eq. (7), the effective resistance depends on the number of strips used in the layout. Its contribution is here minimized by dividing the width of the input transistor in  $n = 60$  strips, giving an effective resistance of 1.5  $\Omega$ . The strips are also connected at both ends in order to avoid increasing its resistive gate noise contribution by four [5].

For the given peaking time, one can see that the ENC is proportional to the total input capacitance  $C_T$  and increases with the square root of the total series resistance  $R_s$ . Calculations give here a noise of 468 electrons (Fig. 4). Thus, for noise optimization it is important to keep this resistance as low as possible.

Eq. (4) gives the thermal noise associated with the feedback transistor  $M_f$ , where  $R_f$  is the equivalent resistance. This noise contribution is inverse proportional to the value of the feedback resistance and proportional to the shaping time constant  $\tau_s$ . The highest resistance value compatible with the requirement in terms of signal pile-up was chosen. Calculations convert this resistance into a typical noise of 75 electrons (Fig. 4).

Concerning the input transistor M1 of the CSA, its noise contribution is dominated by two components, the thermal noise generation in the channel and the flicker noise given by Eq. (5) and Eq. (6), respectively. Due to the peaking time (190 ns) it is anticipated here that the thermal noise is the dominant noise source. It is seen that its thermal noise contribution is proportional to the total input capacitance  $C_T$  and inverse proportional to the square root of its transconductance  $gm$ . Therefore, in order to reduce the thermal noise, the transconductance  $gm$  of the input transistor M1 has to be increased. A calculated thermal noise contribution from M1 of about 238 electrons is achieved here (Fig. 4).

The second noise source in the input transistor M1 given by Eq. (6), is the

flicker (1/f) noise. This noise is inverse proportional to the gate area of the input transistor, strongly dependent on the technology process and independent on the peaking time. The calculation shows that a flicker noise contribution of 4 electrons (simulation shows a contribution of about 20 electrons) is reached (Fig. 4).

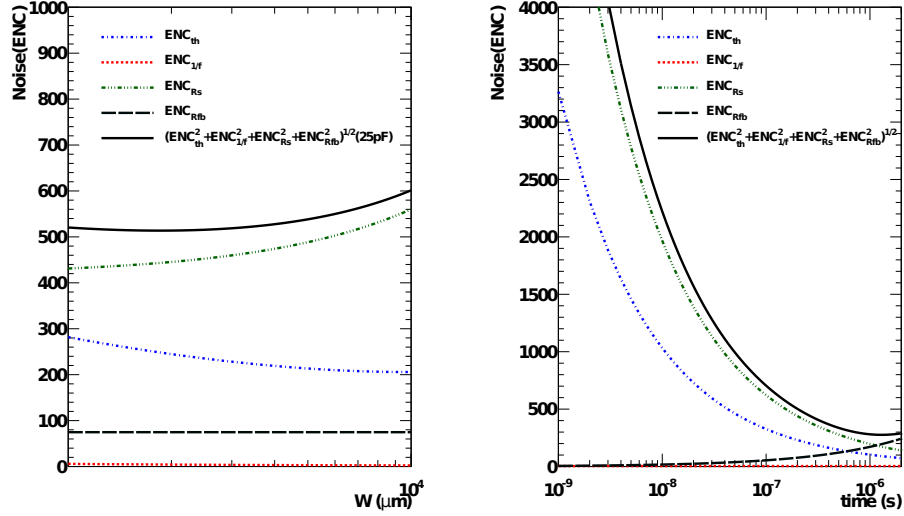


Figure 4: The theoretical optimum noise level as function of width (left) and as a function of the peaking time (right). The four most important sources are quantified individually.

Since all the considered noise sources discussed above are uncorrelated, the total  $ENC_T$  can be obtained by quadratically summing all the individual contributions:

$$ENC_T^2 = ENC_{th}^2 + ENC_{\frac{1}{f}}^2 + ENC_{Rfb}^2 + ENC_{Rs}^2. \quad (8)$$

Figure 4 shows the ENC contribution of each noise source, as well as the total  $ENC_T$  (solid line) plotted as a function of the width (left), and as function of the peaking time (right). From these plots it is clearly seen that the two most dominate noise sources are the series resistance  $R_s$  from the ESD network and the thermal noise of the input transistor M1. The ESD protection resistance  $R_s$  alone, increases the overall noise of the PASA from 248e@25pF to 530e@25pF. Obviously, the best noise performance is achieved without any protection, but the risk of damage will be much higher.

The dependence of the different noise sources with the peaking time was also studied (Fig 4, right). The optimum  $ENC_T$  (solid line) was found to have a theoretical minimum at about 260 electrons with a shaping time of 1000 ns,

but this parameter was fixed to 190 ns by the requirement.

As seen in Fig 4 (left), given the total capacitance of 25 pF and a peaking time of 190 ns, and a current  $I_d$  of 1.5 mA, a value of 2400/0.3 was chosen for W/L of the CSA input transistor. This gives a good noise performance and fulfills the ALICE TPC requirements.

#### 4. The shaper network

The function of the shaper network is to limit the bandwidth of the output signal, in order to avoid aliasing in the subsequent digitization process, and at the same time it has to optimize the overall signal-to-noise ratio. These objectives are achieved by a semi-Gaussian shaper, which is implemented with two low-pass filter stages. Each stage consist of two second-order bridged-T filters connected in cascade as shown in Fig. 5 and Fig. 6.

The first filter generates the first two poles and one zero in the low-pass filter chain. The  $V_{gs}$  of the input transistor of the first shaper was kept equal to the  $V_{gs}$  of the M1 transistor in the CSA, such that the effect of process, temperature and supply voltage variation is largely mitigated. In this context, the first shaper (Fig. 5) is a scaled-down version as the CSA. In order to provide the second shaper with a differential mode input, and to track the DC level variations of the first shaper caused by the unavoidable variations of process parameters and operating conditions, a copy of the first shaper connected in unity gain configuration was implemented. This part has a combined power consumption of 1.43 mW and an open-loop gain of 75 dB.

The second shaper (Fig. 6) consists of a fully differential amplifier with a folded cascode configuration and a CMFB network. It has the same functionality as the first shaper, namely, to implement two other poles and a zero. Together with the differentiator CR-stage and the first shaper stage, it creates the CR-(RC)<sup>4</sup> semi-Gaussian filter.

A continuous time CMFB network (Fig. 6) was implemented to prevent the output of the fully differential amplifier from drifting to either of the two power supplies. This establishes a stable common-mode voltage  $V_{CM}$  of 1.056 V at the output of the second shaper.

The chosen CMFB network (Fig. 6) consists of a resistor/capacitor network applied at the input of the CMFB network. This configuration takes the average of the two outputs,  $V_{out+}$  and  $V_{out-}$ , and compares it with an externally given voltage  $V_{CM}$ . Any deviation of the average value of the two output voltages  $V_{out+}$ ,  $V_{out-}$  with respect to  $V_{CM}$  is sensed and fed back through  $V_{CMFB}$  to the second shaper and corrected for. This scheme ensures a fully balanced output over a voltage range limited by the Common-Mode Range (CMR) of the two non-inverting amplifiers and the source follower of the second shaper.



## 5. The non-inverting stages

The purpose of this stage is to adapt the DC voltage level of the PASA outputs to the input DC levels of the ALTRO. The DC level  $V_{OUT+}$  and  $V_{OUT-}$  is set to 0.56 V and 1.56 V for  $V_{OUT+}$  and  $V_{OUT-}$  respectively by means of the external bias voltages  $V_{REFN}$  (0.56 V),  $V_{REFP}$  (1.56 V), and  $V_{CM}$  (1.056 V).

The last stage in the PASA chain (Fig. 7) consists of a pseudo-differential amplifier implemented by a parallel connection of two equally designed Miller compensated amplifiers each with a gain of 2. This circuit operates in the non-inverting mode, and it uses a low impedance reference voltage  $V_{REFP/N}$ , to offset the output.

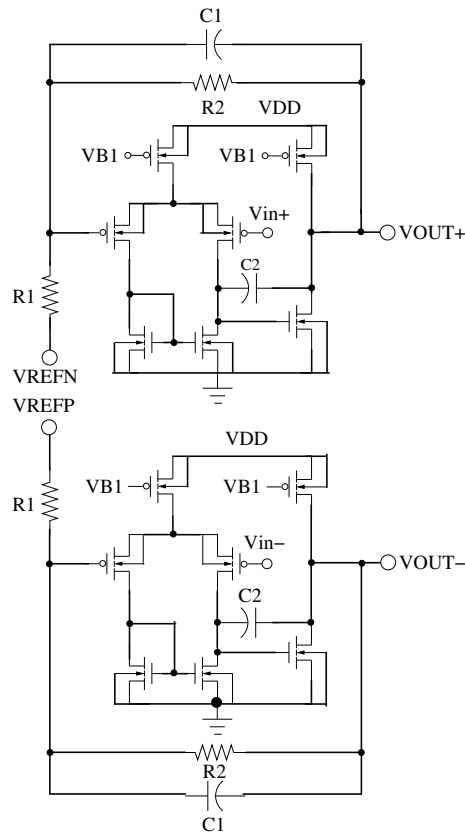


Figure 7: Schematic of the two non-inverting stages.

These two stages have the possibility to change the output levels, independently from each other, according to the following equations

$$V_{OUT+} = \left(1 + \frac{R2}{R1}\right)V_{in} - \frac{R2}{R1}V_{REFN} \quad (9)$$

and

$$V_{OUT-} = \left(1 + \frac{R2}{R1}\right)V_{in} + \frac{R2}{R1}V_{REFP} \quad (10)$$

To prevent potential noise entering the reference path, the external reference voltages VREFP, VREFN and VCM are internally decoupled with 120 pF each.

## 6. The threshold reference self-biased-network

All internal reference voltages of the PASA circuit are generated by a "threshold reference" self-biased network (Fig. 8) is used as a bias for the PASA. It consists of a start-up circuit, a threshold reference self-biased circuit and a chain of current sources for both NMOS and PMOS transistors. The start-up circuit provides a current to the reference circuit through M5 and, as soon as the reference circuit is operating in the desired operation condition, the transistor M5 turns off, and it will not draw any current under normal operation [6].

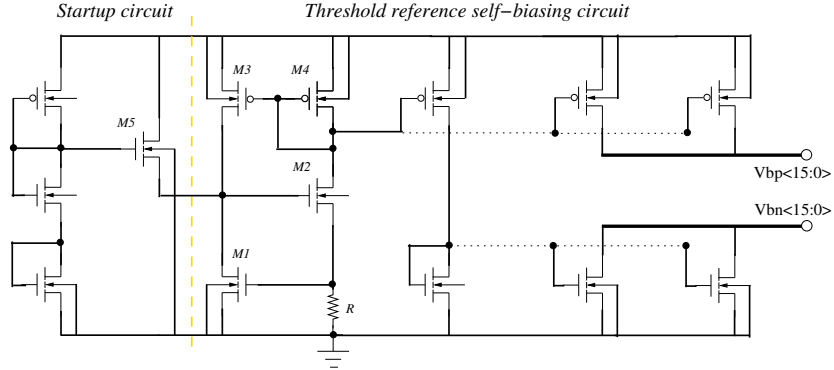


Figure 8: Schematic diagram of the modified threshold reference self-biasing circuit.

To avoid any resistive voltage drop across the width of the chip the distribution of the bias voltages is done by 32 reference currents distributed over the 16-channels. The bias current is then channeled through a diode connected transistor at each bias point to provide locally the bias voltages for the individual transistors.

The threshold self-biased network is placed in the center of the chip (see Fig. 9).

## 7. Layout and floor-planning

To realize a high quality PASA it is very important to take care of the matching and noise issues. Hence, the common-centroid layout technique was used

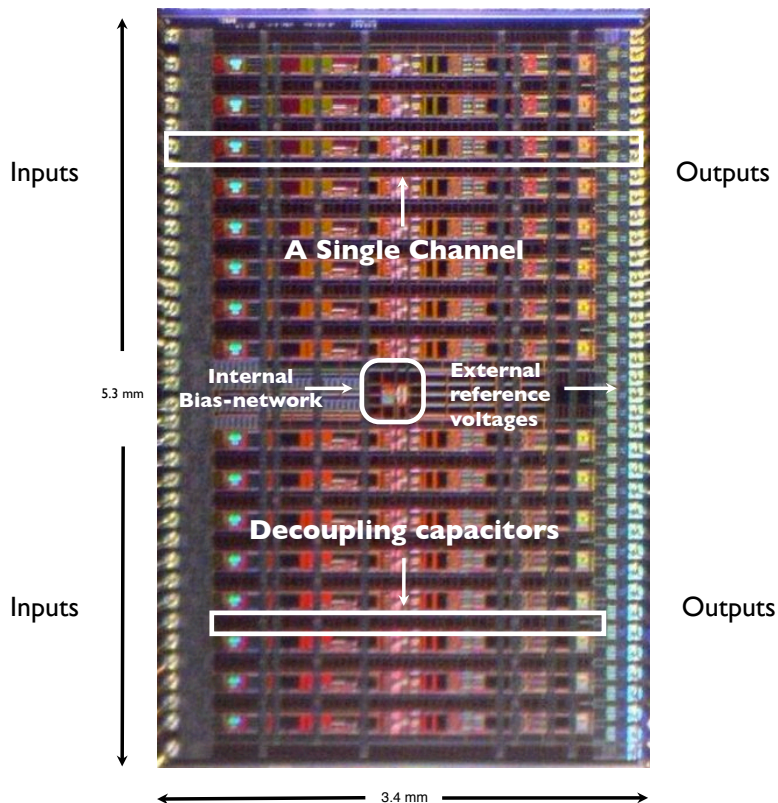


Figure 9: A picture of the produced ALICE TPC PASA.

for parallel and equally sized transistors to avoid errors caused by the gradient effects across the chip, such as temperature, stress and gate-oxide thickness. To minimize the possible mismatch induced by etch undercutting during fabrication, dummy poly strips were used for resistors, capacitors and transistors. As mentioned in subsection 3.1, a finger structure is used for the input transistor M1 to reduce the poly gate resistive noise. This structure also has lower  $C_{bs}$  (bulk-source capacitance) and  $C_{bd}$  (bulk-drain) capacitances and it is convenient for laying out a MOSFET with large W/L ratio [5].

Since noise can couple into the bias nodes and in order to avoid that large signals parasitically couple into the more sensitive analog parts, all bias voltages, especially at the CSA part, are heavily decoupled/filtered to reduce the amplitude of the noise and to keep the internal cross-talk to a minimum.

After the main layout was finished, all free space was filled with substrate

contacts, to both the substrate and the wells.

A picture of the PASA layout is shown in Fig. 9. It has 16 input, 32 output, 16 GND pins, 8 VDD pins and 3 input pins for the reference voltages. The input and output pins are distributed along the length of the chip. The 16-channels, divided in two groups of 8 channels are placed on each side of the threshold self-biased bias network, seen at the center of the chip. The decoupling capacitors together with pads connected to ground are placed adjacent to each channel, creating a physical distance between the channels that helps reducing the cross-talk. In addition each channel is surrounded by a guard ring connected to the substrate which isolates them from each other and further helps to reduce cross-talk.

The final layout of the TPC PASA has a width of 5.3 mm and a length of 3.4 mm, giving a total area of 18 mm<sup>2</sup>.

## 8. Functional analysis prior to submission using simulation

In this section the result of the most relevant simulations are illustrated. They all refer to simulations performed on the circuit back-annotated with the parasitic capacitances extracted from the circuit layout, with an input capacitive load of 25 pF and an input charge of 165 fC. In the design optimization phase, special emphasis was put on understanding the circuit behavior for different process parameter, temperature and voltage changes. The simulated typical PASA impulse response is shown in Fig. 10 and Fig. 11, which illustrate each of the two output signal polarities (VOUT+ and VOUT-) and the differential one respectively. The simulations show the following circuit features: a peaking time of 190 ns, a full width half maximum (FWHM) of 217 ns, a conversion gain of 12.7 mV/fC for the combined outputs, a return to the signal baseline within 550 ns and no undershoot. Under the same simulation conditions the circuit features an equivalent noise charge (ENC) of about 600 electrons.

It should be noticed that the total capacitance at the circuit input influences the noise, the peaking time and the conversion gain.

In the case of the ALICE TPC the capacitance at the PASA input can vary from a minimum of about 10 pF to a maximum of about 25 pF. This includes the contribution from the pad plane and the flexible cable that connects the pad plane to the front-end card (1-20 pF), PCB traces on the front-end card (1-3 pF), and from the package capacitance of about 2 pF. This capacitive spread from 10 to 25pF converts into a variation of the conversion gain from 13.3 mV/fC to 12.74 mV/fC and peaking time variation from 181 ns to 190 ns, is due to the reduction of the bandwidth of the CSA. The pulse amplitude as a function of the detector capacitance has been evaluated and is shown in Figure 12.

Fig. 13 shows the signal response of the common-mode voltage VCM when changed externally +/- 320 mV around 1.060 V. No deviation of the signal is seen.

Fig. 14 shows the signal response and DC response of VOUT+ as a function

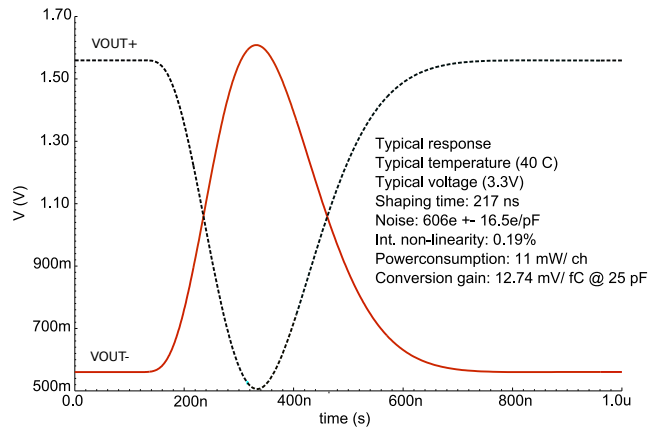


Figure 10: A typical impulse response of the PASA for an input charge of 165fC. The curves for VOUT+ (dashed) and VOUT- (solid) are shown. The baseline voltage of VOUT+ and VOUT- are 1560 mV and 560 mV, respectively.

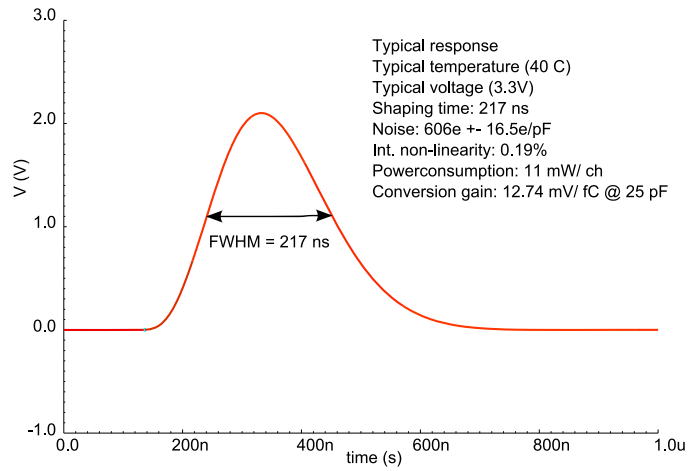


Figure 11: A typical simulated differential pulse response of the PASA for an input charge of 165 fC.

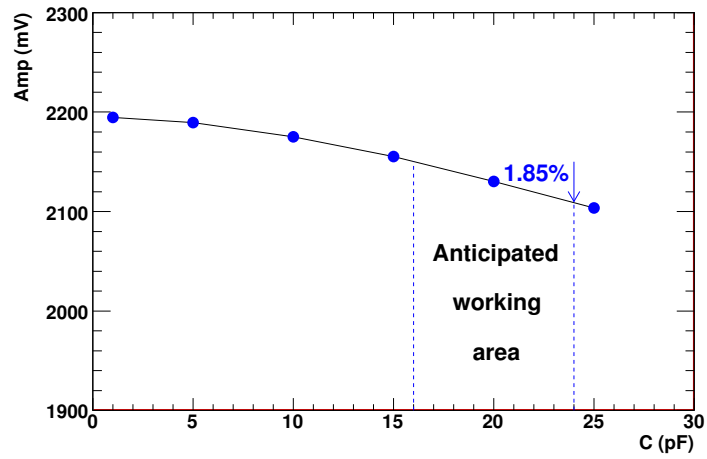


Figure 12: Amplitude variation of the PASA impulse response as a function of total detector capacitance.

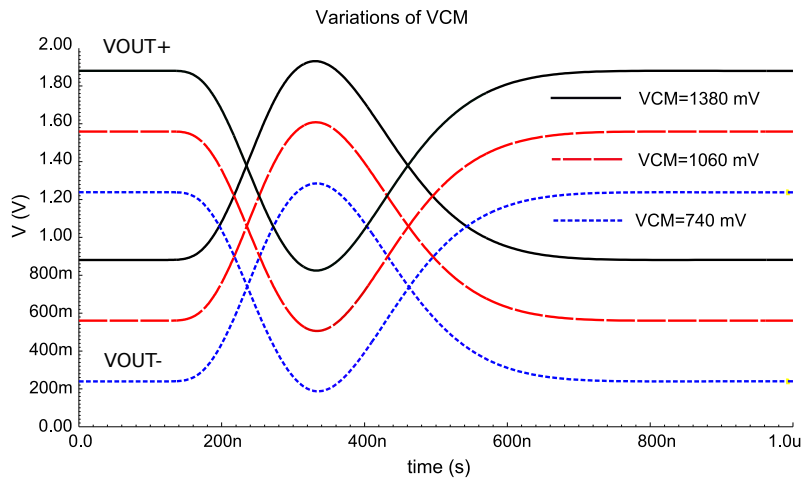


Figure 13: DC output level variation of VOUT+ and VOUT- due to variation of VCM.

of VREFN. A shift VREFN from 400 mV to 760mV was implemented. The circuit responded as given by Eq. 9 and Eq. 10. Also here, no deviation from typical response is observed.

Fig. 15 shows the signal response of the common-mode voltage when changed externally +/- 320 mV around 1.060 V. No deviation of the signal is seen.

The DC levels at the output of the PASA, VOUT+ and VOUT-, are controlled by three externally given reference voltages (VREFP, VREFN and VCM). The response at the output of the PASA when VCM is varied between 740 mV and 1380 mV is shown in Fig. 13. Except for the expected common-mode change, no change in conversion gain and peaking time was seen.

The variation of the manufacturing process parameters causes the variation of the circuit electrical parameters, e.g. the values of transistor threshold, resistor and capacitors. Therefore, one of the challenges in analog chip design is to ensure that the unavoidable variations of the circuit electrical parameters do not lead to an excessive variation of its functional parameters (e.g. conversion gain, peaking time, power consumption and noise).

How this has been achieved in the design of the ALICE TPC PASA is described in section 7. The simulation results for the worst case variation of the foundry manufacturing process parameters is shown in Fig. 16 and (Table 2).

Parameter	Specific.	Simulated
Noise	< 1000e	$\approx 600e(25pF)$
Shaping time [ns]	190	217
Non-linearity	< 1%	0.19%
Crosstalk	< 0.3%	-
Baseline variation	-	-
Conv. gain [mV/fC]	12	12.7@25pF
Powercon.[mW/ch]	< 20	11

Table 2: Compilation of the simulation results of the main parameters compared to the specifications.

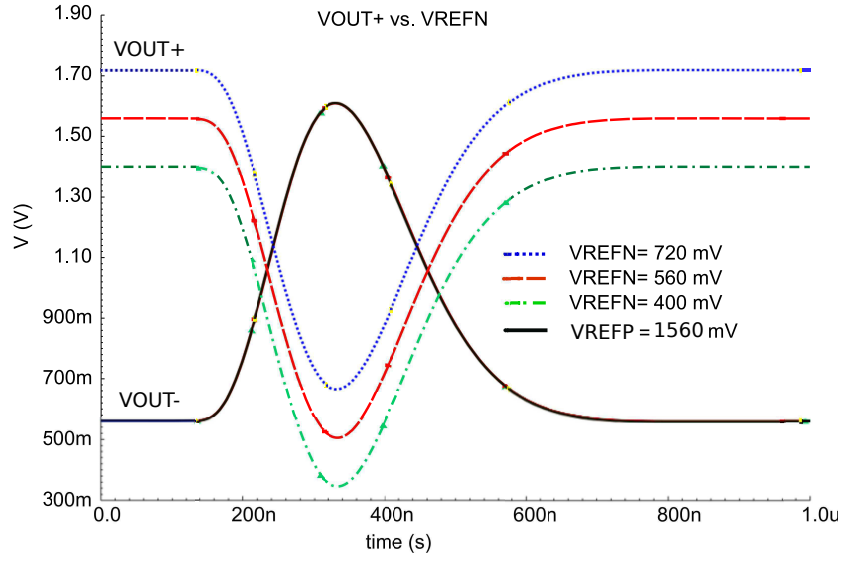


Figure 14: DC output level variation of  $V_{OUT+}$  due to variation of  $V_{REFN}$ .

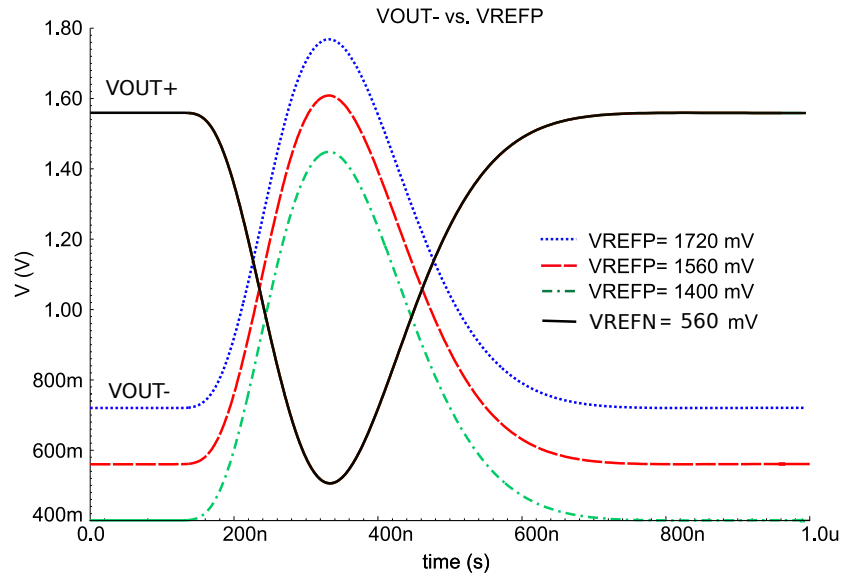


Figure 15: DC output level variation of  $V_{OUT-}$  due to variation of  $V_{REFP}$ .

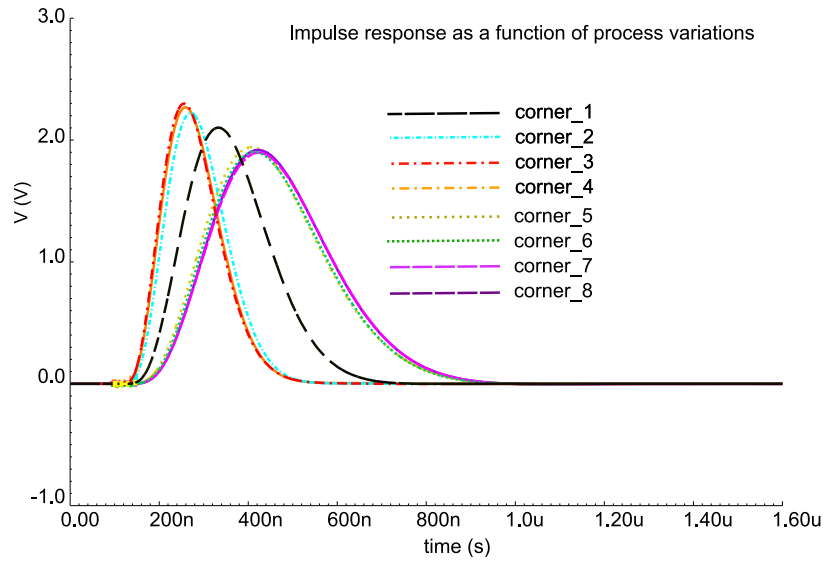


Figure 16: PASA impulse response for the eight recommended corner combinations by AMS.

## 9. Measurement results and system behavior

In order to qualify the ALICE TPC PASA the necessary test equipment was developed and built at the Technische Universität Darmstadt (TU-Darmstadt, Germany) and at the Lund University (Sweden). A comprehensive description of the test setup can be found in [7]; only a short explanation of the test procedure will be given here.

The functionality of the chip is characterized by injecting a charge generated by a 14-bit DAC placed on the test board into the 16 PASA inputs, one at the time. The full set of tests for all 32 outputs signals were performed for 3 values of the supply voltages (3.0, 3.3 and 3.6 V). The PASA output signals were then converted by a 12-bit 40-MSPS ADC. From these measurements the following values were extracted: the power consumption, the conversion gain, the peaking time, the noise and the linearity. Initially the static power consumption was measured. If the power test fulfills the acceptable power consumption region, the test continue, if not, the test was terminated and the chip was characterized as non-functional.

Since the ALICE TPC PASA was adopted for the upgrade of the STAR TPC at the Brookhaven National Laboratory (BNL), and went through exactly the same test procedure, the results obtained for both the 47637 ALICE TPC PASA chips and for the 22795 chips from the STAR TPC production are presented here.

In subsection 9.2 the system behavior of the ALICE TPC PASA is shown.

### 9.1. Measurement results

Figure 17 shows the first measured output pulse shape on one engineering sample of the ALICE TPC production. The measurement was done on a fully equipped front-end board for a single channel of a randomly chosen chip. For an input charge of 150 fC the conversion gain is 12.7 mV/fC, the peaking time is 160 ns and the FWHM is 190 ns. This pulse is fitted with the ideal gamma-4 response function and shows an almost perfect matching with the measured waveform. The channel integral non-linearity was found to be 0.2% over the full dynamic range of 150 fC, less than the 1% given by the specifications. The single channel had a noise value below 570 e (r.m.s.) for an input capacitance of 12 pF, and a channel-to-channel cross-talk was below -60 dB.

The general performance of the full custom PASA chip is listed in Tab. 3, and the distribution of the key parameters are

presented in Figure 18. For the ALICE TPC PASA an acceptability region of  $\pm 20\%$  from the mean power consumption, in this case of about 187 mW, was defined. A total of 307 chips was found to have a power consumption outside the acceptance region. Of these, 180 chips had a power consumption outside the maximum measurable power consumption of 285 mW, and then characterized as non-functional. The small difference in the average power consumption between the distributions is due to the unavoidable variation in the process parameters from different production lots as discussed in section 8.

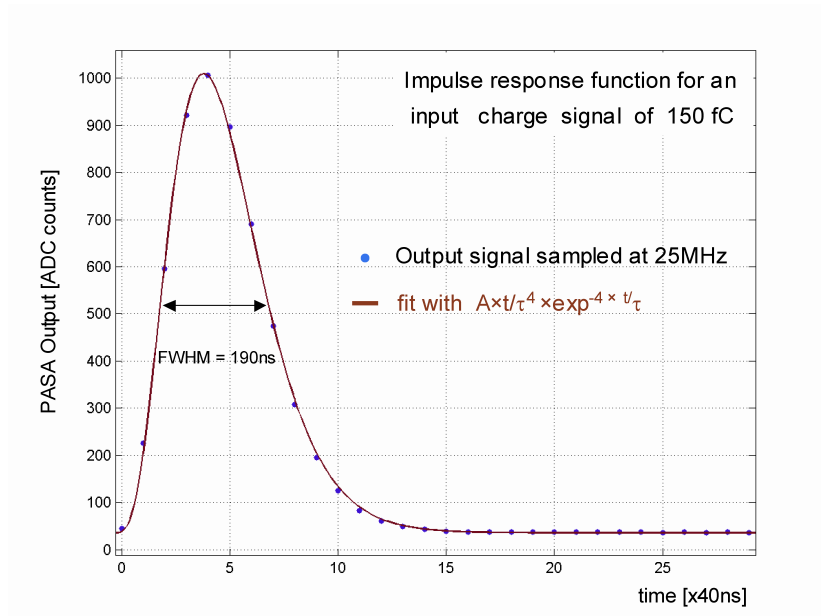


Figure 17: Typical measured response of the ALICE TPC readout electronic. The plot shows a measured output response with an ideal gamma-4 response function.

Conversion gain mean values of 13.4 mV/fC@5 pF, of 13.2 mV/fC@5 pF and of 13 mV/fC@5 pF were found for the engineering run, for the production run and for the STAR upgrade production, respectively, as seen in Figure 18. A small difference in the conversion gain is also seen, as is expected from chips coming from different lots or productions.

The measured peaking time (Fig. 18, top right) is typically around 160 ns, a bit shorter than the expected value from the simulation results. This is a known artefact seen in several Multi-Project Wafer (MPW) runs. Therefore, to cope with this, the circuit was designed with a slightly larger shaping time equal to the deviation experienced from these previous MPW submissions.

Taking into consideration the known deviation in peaking time between simulation and measurement, the measurement results show very good agreement between simulation and measurement. An MPW production of a new chip with similar topology and design strategy done in 2005 [9] does not show this shift in peaking time.

The bi-dimensional plot of the conversion gain versus the power consumption, the peaking time versus the power consumption and the conversion gain versus the peaking time are shown in Fig. 18 also. Relatively good distributions of the conversion gain versus power consumption are seen for the ALICE TPC PASA and for the STAR upgrade productions, and most of the channels show a conversion gain between 12 mV/fC and 14 mV/fC and as expected, it does

Parameter	Specific.	Simulated	Tested
Noise	< 1000e	385e(12 pF)	$\approx$ 385e(12pF)
Shaping time [ns]	190	212(12 pF)	$\approx$ 190
Non-linearity	< 1%	0.19%	0.2%
Crosstalk	< 0.3%	-	<0.1%
Baseline variation	-	-	+80mV
Conv. gain [mV/fC]	12	12.74@25pF	$\approx$ 12.8@12pF
Powercon.[mW/ch]	< 20	11	11.67

Table 3: Summary of the simulated and tested values of the ALICE TPC PASA.

not show any visible correlation with the power consumption. Since the STAR upgrade production consists of a single lot of 25 wafers, it shows a narrower distribution than that for the ALICE production, which consist of two lots of 25 wafers. The same is also observed for the individual lots for the ALICE TPC PASA productions. Very few chips are outside the acceptance region.

The peaking-time versus the power consumption shows a weak correlation for the ALICE TPC PASA and no correlation for the STAR upgrade production. The reason is clearly the shift in process parameters from different productions in the ALICE TPC PASA.

The conversion gain versus peaking time shows similar behavior as the previous distribution also due to different productions. Very few chips are outside the acceptance region.

The DC level of the circuit's differential output (baseline), which can be controlled by means of two external bias voltages VREFN and VREP, should be kept at a value sufficiently close to the bottom of the circuit's dynamic range, in order to preserve the maximum dynamic range. Since VREFP and VREFN will be common to all channels in one front-end card (or possible for all front-end cards in the whole detector), it is important to verify the dispersion of the circuit output baseline for given values of the external bias voltages VREFP and VREFN. This is shown in Fig. 19. For the ALICE TPC PASA, these distributions are Gaussian like up to  $\pm 4.2 \sigma$ , while for STAR upgrade the distribution of VOUT+, VOUT-, and VOUT+-VOUT- are Gaussian up to

$\pm 5 \sigma$ . The number of channels outside the same acceptance region as for the the ALICE TPC PASA,

In the bottom row left and right the correlation between VOUT+ and VOUT- is shown for ALICE TPC PASA and STAR upgrade PASA production respectively. These plots show a very good correlation between the two output voltages.

Table 4 and Table 5 show a summary of the most relevant results of the mass production test of the PASA for the ALICE TPC and the STAR upgrade, respectively.

Taken into account the acceptable region of operation, as discussed above, a

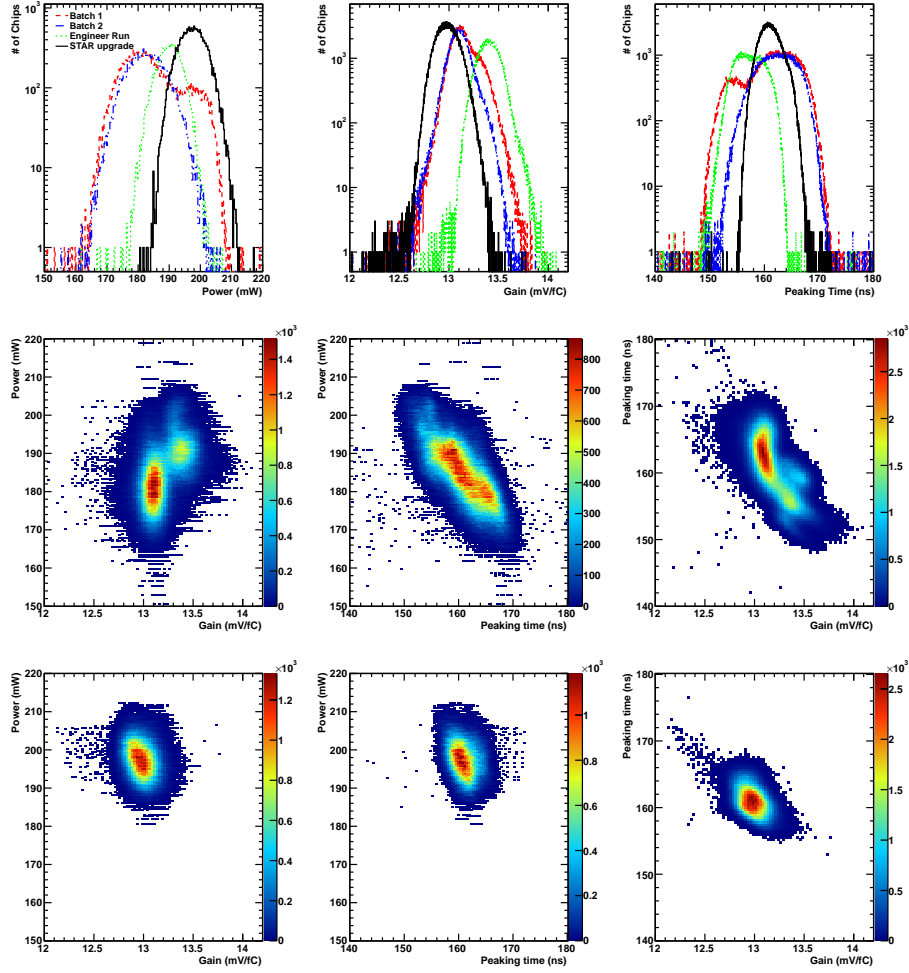


Figure 18: Distribution of the power consumption (top left), conversion gain (top right) and peaking time (top right) for the engineering run (dotted), the two batches from the ALICE TPC PASA production (dashed and dashed-dotted), and the total STAR TPC chip upgrade production (solid). Middle and bottom rows show from left to right the power versus conversion gain distribution, the power versus peaking time and the peaking time versus conversion gain for the ALICE TPC PASA and for the STAR upgrade production, respectively.

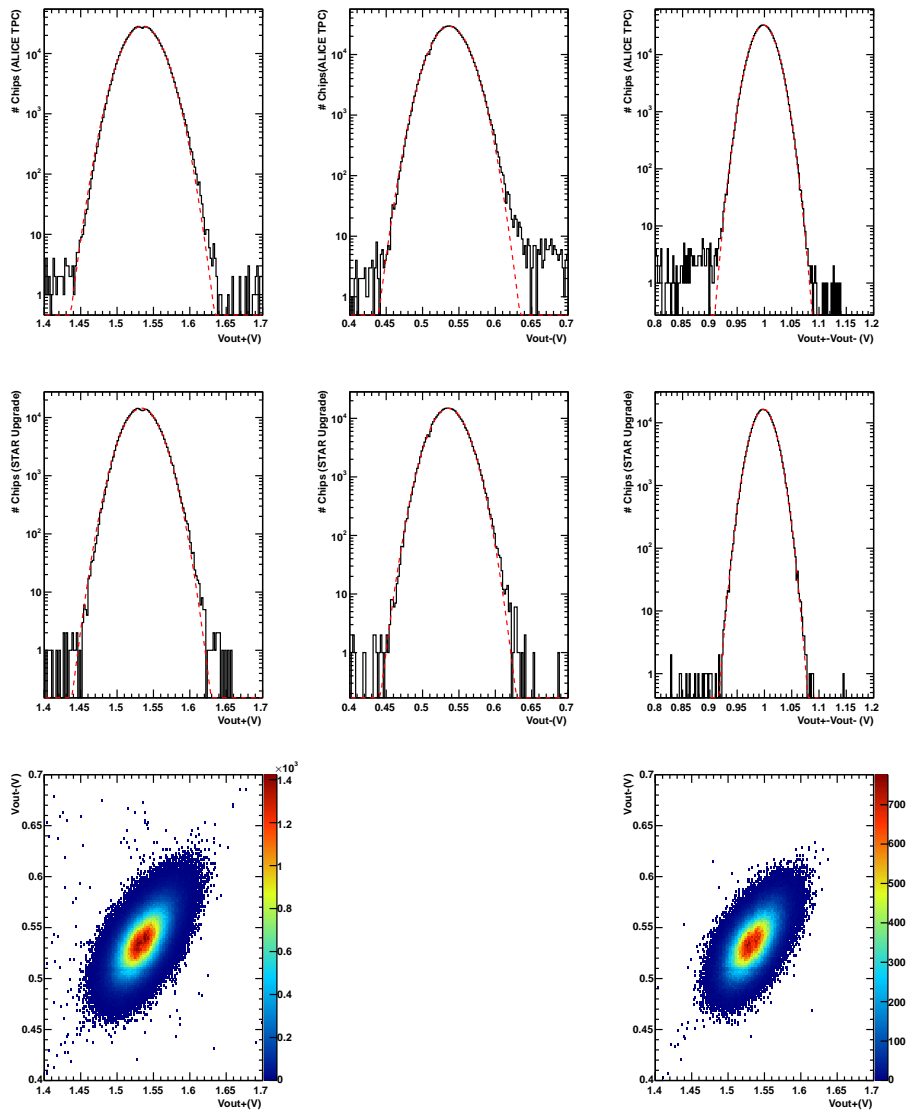


Figure 19: The top and the middle rows show the distribution of  $V_{OUT+}$  (left),  $V_{OUT-}$  (middle) and  $V_{OUT+} - V_{OUT-}$  (right) for the ALICE TPC PASA and for the STAR upgrade production, respectively. The dashed line shows a Gaussian fit to the distributions. In the bottom row the correlation of  $V_{OUT-}$  versus  $V_{OUT+}$  is shown for ALICE TPC PASA (left) and STAR upgrade production (right).

Non accepted	ALICE frequency			
	Channels		Chips	
	#	%	#	%
None			46 585	98
Power (20%)			307 (180)	0.65
Conv. gain (8%)	4922 (2880)	0.65	914	1.9
Peaking time (10%)	4492 (2880)	0.59	673	1.4
VOUT+ (80 mV)	2498 (1630)	0.33	654	1.4
VOUT - (80 mV)	2290 (1553)	0.3	593	1.2
VOUT+ - VOUT - (80 mV)	2297 (1466)	0.3	633	1.3
Total amount of Chips			1052	2.2
Total			47 637	100.0

Table 4: Acceptance levels for the PASAs as chosen for the ALICE TPC.

Non accepted	STAR frequency			
	Channels		Chips	
	#	%	#	%
None			22 609	99.2
Power (20%)			63 (35)	0.3
Conv. gain (8%)	2037 (560)	0.55	160	0.7
Peaking time (10%)	2014 (560)	0.55	137	0.6
VOUT+ (80 mV)	376 (231)	0.10	113	0.5
VOUT - (80 mV)	320 (205)	0.09	101	0.4
VOUT+ - VOUT - (80 mV)	375 (228)	0.10	111	0.5
Total amount of Chips			181	0.80
Total			22 795	100.0

Table 5: Acceptance levels for the PASAs as chosen for the STAR TPC.

total of 1052 chips were found to be outside this region (mostly due to one channel). This gives a production yield for the ALICE TPC PASA of nearly 98%. For the STAR upgrade production, the number of chips outside the acceptance region, the same as for the ALICE TPC PASA, was 186. This corresponds to a yield of 99.2%.

### 9.2. System measurements

In this section we illustrate the performance of the PASA, with special focus on the noise, as measured on the ALICE TPC fully instrumented with the electronics.

Fig. 20 shows the measured system noise performance in ENC as a function of the x versus y position in the A-side and in the C-side of the ALICE TPC detector. As mentioned, each sector in the A-side and C-side consist of three different pad sizes. The ENC distribution for each of the three pad sizes separately and the overall noise distribution is shown in Fig. 21. The noise spread between the channels, which shows a very systematic pattern is mainly due to the difference in trace length on the chamber pad plane and to the different trace length on the front-end board. Measured and extracted values given by the system measurement are summarized Tab. 6.

Parameter	IROC	OROC1	OROC2
Trace length (cm)	120	120	150
ADC- counts/cm	0.21	0.22	0.23
Pad capacitance (pF)	6-10	6-10	6-10
FEE capacitance (pF)	3-5	3-5	3-5
Noise ADC-counts (without traces)	0.589	0.603	0.624
Noise ADC-counts (with traces)	0.67	0.7	0.78
Noise in electrons (without traces)	570	584	604
Extracted capacitance (pF)	11-13	11-14	12-14
Extracted Average capacitance (pF)	18	21	26
Extracted noise slope (1.3 pF/cm assumed)	15.6	15.2	15.9

Table 6: The seven first rows are values given by the system measurement [8]. The three last rows are extracted values.

An overall typical mean noise of 0.71 ADC counts was here achieved. This converts into an ENC equal to 710 electrons and is very close to optimum of what we can expect from a system of this complexity. This value corresponds to an average system capacitance of about 21 pF.

The total measured system noise for the IROC, for the OROC1 and for the OROC2 as a function of the total detector capacitance is shown in Fig. 22 (full-lines). After subtracting the ADC noise contribution of 420e ( $PASA = \sqrt{total^2 - ADC^2}$ ), the noise contribution from the ALICE TPC PASA can be

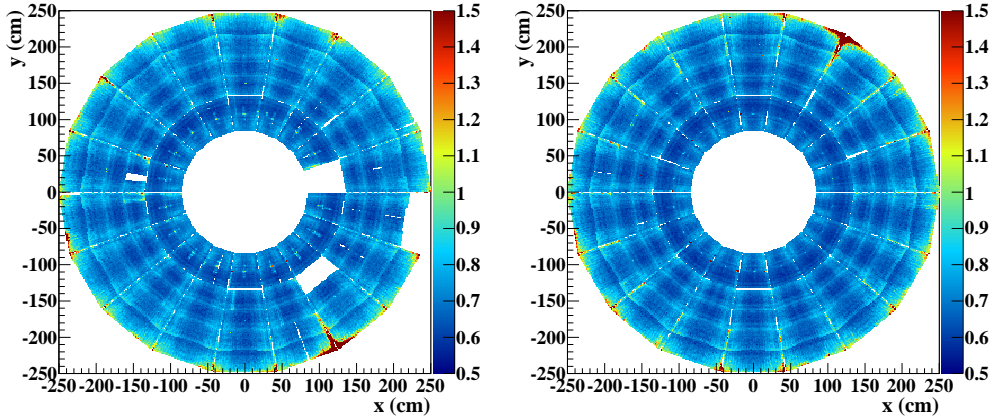


Figure 20: Measured system noise for the A-side (left) and C-side (right) of the ALICE TPC detector [8].

compared with the simulated one (dashed lines in Fig. 22). The measured noise is found to be, as expected, a little larger than the simulated value.

## 10. Conclusions

This paper describes the full custom design of the ALICE TPC PASA. Simulation results of the layout with extracted parasitics done prior to the submission of the chip have been presented. About 48000 chips, with a total of about 762 176 channels have been fabricated and fully tested. Theoretical calculation, simulation and system measurements results show very good agreement with each other. The ALICE PASA production has successfully satisfied all specifications with good margin. In particular, the evaluation of the noise in the fully commissioned system shows an ENC noise behavior of typically 0.71 ADC-counts (710 electrons). This is close to optimum of what we can expect for such a complex system including both PASA, ADC (ALTRO) and other electronics placed in the vicinity of the ALICE TPC PASA.

A baseline shift and a small offset in power consumption is seen, due to manufacturing variations that will result in process and device parameter variations from lot-to-lot, wafer-to-wafer, die-to-die, and device-to-device.

The extreme chip and system tests show a yield of about 98%. Losses are mainly due to one channel being outside the acceptance region. This very high yield is the result of a robust design optimized using extensive simulations, including extracted parasitics from layout, for the recommended AMS corners, and of the techniques used in the layout to reduce the effect of the process variations. The circuit was realized in AMS's C35B3C1 0.35  $\mu\text{m}$  CMOS process, has a area of 18  $\text{mm}^2$  and the die is packed in a TQFP 144 package.

The ALICE TPC PASA has been selected for the upgrade at STAR TPC

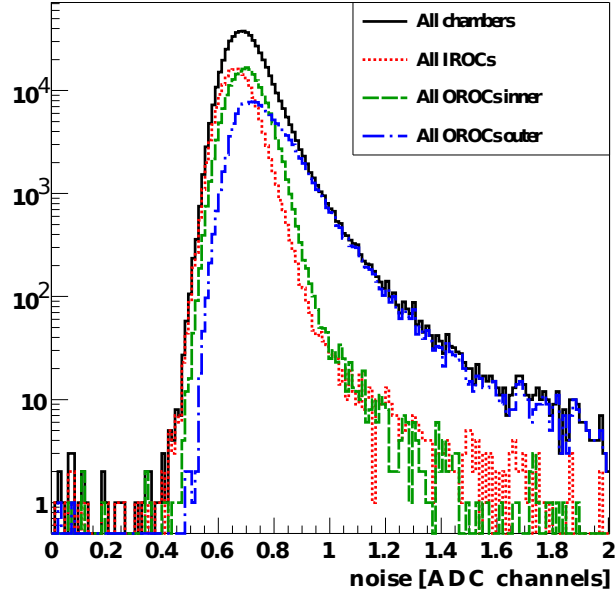


Figure 21: The distribution of the overall system noise in the final setup in the ALICE experiment. The histogram for the three pad sizes and the overall noise histogram are shown [8].

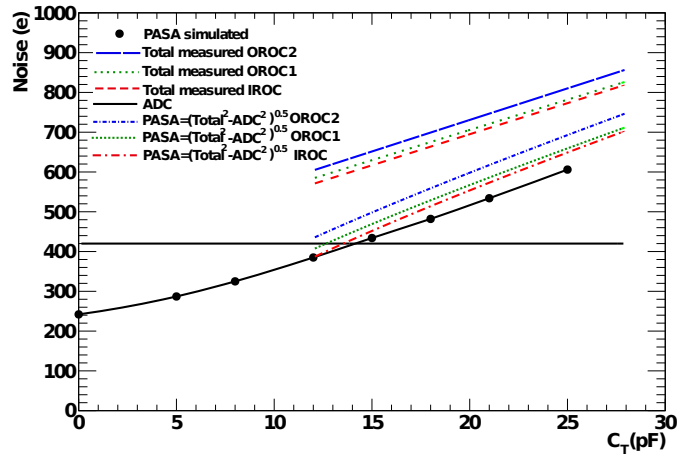


Figure 22: Noise versus the total capacitance  $C_T$ .  $C_T$  varies from 12 to 28 pF with a mean value around 21 pF.

(11500 chips), it also being used at MIPP/Fermilab (1100 chips) and at BONUS/JLAB (a few hundred chips).

## 11. Acknowledgement

We would like to thank BMBF for the financial support of this project. We also thank Marcus Dorn for his IT support and maintainance of the Cadence system. We also thank Kjetil Ullaland for valuable comments to this manuscript.

## References

- [1] K. Aamodt et al. (the ALICE Collaboration), “The ALICE experiment at the CERN LHC”, *Journal of Instrumentation* 3 (2008) S08022.
- [2] R. Esteve Bosch, A. Jimenez, B. Mota and L. Musa, “The ALTRO Chip: A 16-Channel A/D Converter and Digital Processor for Gas Detectors” *IEEE Transactions on Nuclear Science*, Vol 50 No.6 December 2003.
- [3] G. De Geronimo, P. O’Connor, *Nuclear Instruments and Methods in Physics Research A*421 (1999) 322.
- [4] G. Gramegna, P. O’Connor, P. Rehak, S. Hart, *Nuclear Instruments and Methods in Physics Research A*390 (1997), 241-250.
- [5] Z.Y. Chang and W.M.C. Sansen, “Low-noise wide-band amplifiers in bipolar and CMOS technologies”, Kluwer Academic Publishers, 1991.
- [6] R. Jakob Baker, “CMOS circuit Design, Layout, and Simulation”, A JOHN WILEY & SONS, INC., PUBLICATION.
- [7] U. Bonnes, H. Oeschler and the ALICE Collaboration. “Testing of the PASA Chips of the ALICE TPC”, GSI Annual Report 2004. INSTMETH-18.
- [8] J. Wiechula, Private communication.
- [9] H.K. Soltveit, “Preamplifier-shaper prototype for the Fast Transistion Detector of the Compressed Baryonic Matter (CBM) experiment at FAIR” 12th Workshop on Electronics for LHC and Future Experiments. (2006) 520.